The Ground State of the Pseudogap in Cuprate Superconductors

The Ground State of the Pseudogap in Cuprate Superconductors

T. Valla,[1]* A. V. Fedorov,[2] Jinho Lee,[3] J. C. Davis,[3] G. D. Gu[1]

We present studies of the electronic structure of La$_{2-x}$Ba$_x$CuO$_4$, a system where the superconductivity is strongly suppressed as static spin and charge orders or "stripes" develop near the doping level of $x = \frac{1}{8}$. Using angle-resolved photoemission and scanning tunneling microscopy, we detect an energy gap at the Fermi surface with magnitude consistent with d-wave symmetry and with linear density of states, vanishing only at four nodal points, even when superconductivity disappears at $x = \frac{1}{8}$. Thus, the nonsuperconducting, striped state at $x = \frac{1}{8}$ is consistent with a phase-incoherent d-wave superconductor whose Cooper pairs form spin-charge–ordered structures instead of becoming superconducting.

There are several generally accepted phenomena in high-temperature superconductivity (HTSC) that make the cuprates so fascinating. One of these phenomena is a d-wave symmetry of the superconducting gap. Another feature is a normal-state gap (pseudogap) in underdoped materials, which exists above the temperature of the superconducting transition T_C (1, 2). There are multiple aspects to the pseudogap phenomenon. In particular, the distinction is usually made between the "large" pseudogap in the overall density of states (DOS) and a "small" pseudogap in the excitations at the Fermi surface, which is seen in spectroscopic probes such as angle-resolved photoemission spectroscopy (ARPES) (1, 2). Here, we consider the small pseudogap. It is generally believed and observed that the magnitude of the pseudogap monotonically decreases with increasing doping, whereas T_C moves in the opposite direction in the underdoped regime (1, 2). The origin of the pseudogap and its relationship to superconductivity are some of the most important open issues in the physics of HTSC and represent the focal point of current theoretical interest (3–6). In one view, the pseudogap is a pairing (superconducting) gap, reflecting a state of Cooper pairs without global phase coherence. The superconducting transition then occurs at some lower temperature when phase coherence is established (7). In an alternative view, the pseudogap represents another state of matter that competes with superconductivity. However, the order associated with such a competing state has never been unambiguously detected. The first hints came from neutron-scattering studies in a magnetic field, where an incommensurate spin order was detected inside vortices (8). However, it was not until recent scanning tunneling microscopy (STM) experiments that more was learned about any potential candidate for such "hidden

order." A charge-ordered state, energetically very similar to the superconducting state, has been found in the vortex cores (9), in the pseudogap regime (10) above T_C, and in patches of underdoped material in which the coherent conductance peaks were absent (11). We show that a similar state represents the ground state in a system with strongly suppressed superconductivity and with a static spin (12) and charge (13) orders: La$_{2-x}$Ba$_x$CuO$_4$ (LBCO) at doping level $x = \frac{1}{8}$. The k-dependence of the gap in this state looks the same as the superconducting gap in superconducting cuprates: It has magnitude consistent with d-wave symmetry and vanishes at four nodal points on the Fermi surface. Fur

thermore, the single-particle gap, measured at low temperature T, has unexpected doping dependence with a maximum at $x \approx \frac{1}{8}$, precisely where the charge-spin order is established between two adjacent superconducting domes. These findings reveal the pairing origin of the pseudogap and imply that the most strongly bound Cooper pairs at $x \approx \frac{1}{8}$ are most susceptible to phase disorder and spatial ordering (7, 14, 15).

LBCO exhibits a sharp drop in superconducting transition temperature, $T_C \rightarrow 0$, when doped to $\sim\frac{1}{8}$ holes per Cu site ($x = \frac{1}{8}$) (16), while having almost equally strong superconducting phases at both higher and lower dopings, reaching maximal $T_C \approx 32$ K at $x = 0.095$ and $x = 0.155$. Therefore, the $x = \frac{1}{8}$ case represents an ideal system to study the ground state of the pseudogap because the normal state extends essentially to $T = 0$ K. In scattering experiments on single crystals, a static local spin order with period of eight unit cells (12, 14) and a charge order (13) with period of four unit cells— so-called stripes—has been detected at low T. While superconductivity is strongly reduced at $x = \frac{1}{8}$, metallic behavior seems to be preserved. Optical studies have detected a loss of spectral weight at low frequencies with simultaneous narrowing of a Drude component, which suggests the development of an anisotropic gap (17). We used ARPES and STM to measure the electronic excitations and detailed momentum dependence of the single-particle gap in the ordered state of LBCO.
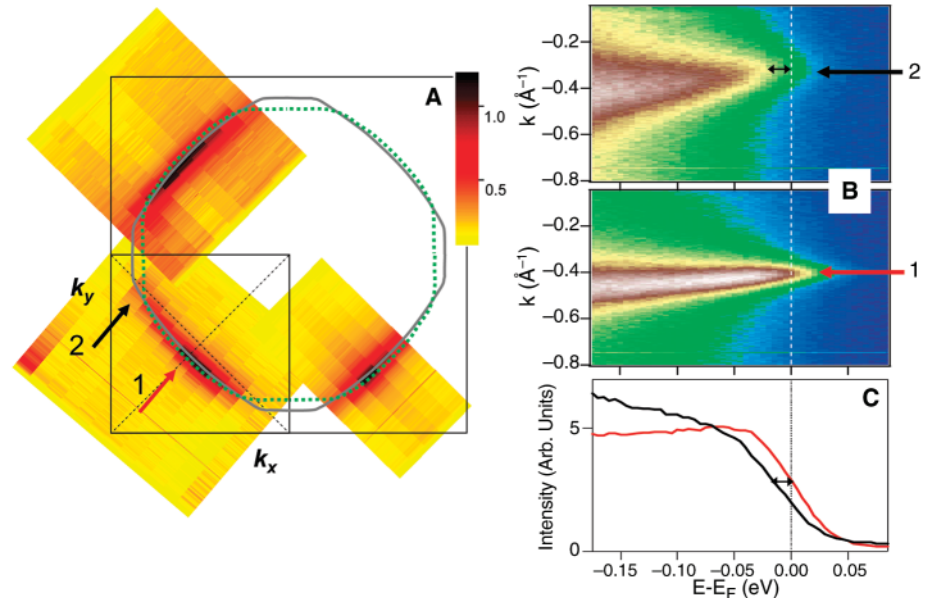

Fig. 1. Photoemission from LBCO at $x = \frac{1}{8}$. (**A**) Photoemission intensity from a narrow interval around the Fermi level ($\omega = 0 \pm 10$ meV) is shown on a relative scale as a function of the in-plane momentum. High intensity represents the underlying Fermi surface. Lines represent fits to the positions of maxima in probed MDCs for LBCO ($x = 0.125$) (solid line) and LSCO ($x = 0.07$) (dashed line). Arrows correspond to the momentum lines represented in (B) and (C). k_y and k_x represent in-plane momenta spanning the Brillouin zone. (**B**) Photoemission intensity from LBCO sample as a function of binding energy along the momentum lines indicated in (A). (**C**) Energy distribution curves (EDCs) of spectral intensity integrated over a small interval $k_F \pm \Delta k$ along the two lines in k-space shown in (B), where $\Delta k = 0.08 \text{Å}^{-1}$. E-E$_F$, is energy measured from the Fermi level. The arrow represents the shift of the leading edge. The spectra were taken in the charge-ordered state at $T = 16$ K.

[1]Condensed Matter Physics and Materials Science Department, Brookhaven National Laboratory, Upton, NY 11973, USA. [2]Advanced Light Source, Lawrence Berkeley National Laboratory, Berkeley, CA 94720, USA. [3]Laboratory for Atomic and Solid State Physics, Department of Physics, Cornell University, Ithaca, NY 14853, USA.

*To whom correspondence should be addressed. E-mail: valla@bnl.gov

Figure 1 shows the photoemission spectra from LBCO at $x = \frac{1}{8}$ in the ordered state ($T = 16$ K). The momentum distribution of the photoemission intensity from the energy window of ±10 meV around the Fermi level is shown within the Brillouin zone (Fig. 1A). From these and other contours measured for several samples, we extracted the Fermi surface as a line in momentum space that connects the maxima of each of the measured momentum distribution curves (MDC) at energy $\omega = 0$. In addition, we also show the extracted Fermi surface of La$_{2-x}$Sr$_x$CuO$_4$ (LSCO) at $x = 0.07$, which agrees well with published data (18). The areas enclosed by the Fermi lines correspond to $x = 0.06 \pm 0.015$, for LSCO and $x = 0.115 \pm 0.015$, for LBCO, in good agreement with the nominal doping levels, signaling that the bulk property has been probed. In both systems, we have detected an excitation gap (19) with a magnitude that depends on the k position on the Fermi surface, vanishing at the node and with maximum amplitude near the antinode as shown in Fig. 1, B and C.

In the detailed k-dependence for several samples (Fig. 2), two unexpected properties are uncovered. First, gaps in all samples have magnitudes consistent with d-wave symmetry even though superconductivity is essentially nonexistent in LBCO at $x = \frac{1}{8}$. Second, the gap in LBCO is larger at $x = \frac{1}{8}$ than at $x = 0.095$ and than in LSCO ($x \approx 0.07$). This finding contradicts a common belief that the excitation gap in cuprates monotonically increases as the antiferromagnetic (AF) phase is approached. Figure 2C shows the compilation of the maximal gap values, Δ_0, in LSCO and LBCO systems, as a function of doping, from this study and from previously published work. Values for LSCO for $x = 0.063$ and $x = 0.09$ are extracted from figure 4 in (18) and those for $x \geq 0.1$ are from (2). All the points have been measured at $T \approx 20$ K: in the superconducting state for $x = 0.09$, 0.095, 0.1, 0.165, and 0.22, and in the normal state for the other samples. It is clear from the figure that the total gap is not monotonic. Rather, in LBCO, it peaks at or near $x = \frac{1}{8}$ when superconductivity vanishes and stripes are fully developed.

The momentum-resolved picture from ARPES is consistent with the STM data obtained from an LBCO sample at $x = \frac{1}{8}$, cut from the same parent crystal used for ARPES. In Fig. 3A, a typical STM topographic image of a cleaved LBCO surface is shown. In addition, the differential conductance (dI/dV) spectra were taken at many points in a wide range of energies (fig. S2). In the averaged (over the whole field of view in Fig. 3A) conductance spectrum (Fig. 3B), a symmetric v-like shape at low energies, with zero-DOS falling exactly at the Fermi level, which is consistent with a pairing d-wave gap. The magnitude of this gap, $\Delta_0 \approx 20$ meV, as determined from the breaks in dI/dV curve agrees with the maximal gap Δ_0 measured in photoemission.

Our study provides the evidence for a d-wave gap in the normal ground state of a cup-

rate material. Previous studies on underdoped Bi$_2$Sr$_2$CaCu$_2$O$_{8+\delta}$ (BSCCO) were always affected by the superconductivity: The disconnected "Fermi arcs" were seen, shrinking in length as T was lowered below pseudogap temperature T^* and collapsing onto (nodal) points below T_C (20, 21). As a result of this abrupt intervention of superconductivity, it was not clear whether the pseudogap ground state would have a Fermi arc of finite length or a nodal point or whether it would be entirely gapped. In LBCO, the absence of superconductivity at $x = \frac{1}{8}$ has enabled us to

resolve this puzzle and to show that the normal-state gap has isolated nodal points in the ground state. This result points to the pairing origin of the pseudogap, in general agreement with recent thermal transport measurements (22). With increasing T, a finite-length Fermi arc forms, as suggested in Fig. 2B, in accord with results on BSCCO (20, 21).

What might be the origin of the observed d-wave gap in LBCO if superconductivity is absent? Neutron- and x-ray–scattering studies on the same crystal have identified a static spin order
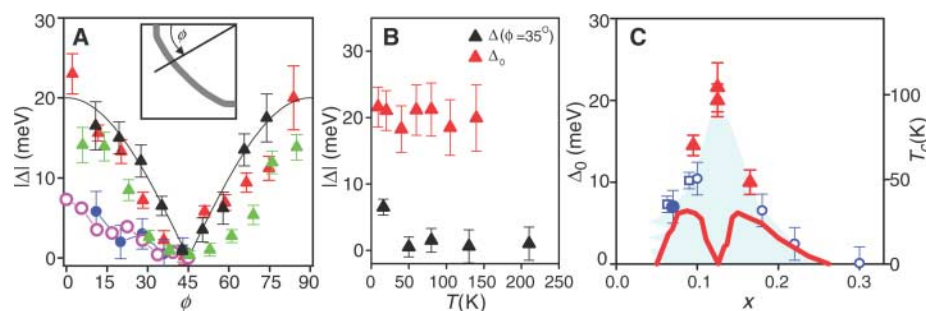

Fig. 2. k- and doping dependence of the single-particle gap. (**A**) Magnitude of single-particle gap (leading-edge gap) at $T = 16$ K as a function of an angle ϕ around the Fermi surface, as defined in the inset, for LBCO at $x = \frac{1}{8}$ (black and red triangles), $x = 0.095$ (green triangles), and LSCO at $x = 0.07$ (blue circles) have been measured. Points for LSCO at $x = 0.063$ (magenta circles) have been extracted from figure 4A in (18). The line represents a d-wave gap amplitude, $\Delta_0|\cos(2\phi)|$ with $\Delta_0 = 20$ meV. (**B**) Temperature dependence of Δ_0 (red triangles) and Δ at $\phi \approx 35°$ (black triangles) for LBCO at $x = \frac{1}{8}$. (**C**) Doping dependence of Δ_0 in LBCO (triangles) and LSCO (circles and squares). Solid symbols, this study; open squares, (18); open circles, (2). The red line represents doping dependence of T_C for LBCO from (16). Error bars in (A) to (C) indicate fitting uncertainty in position of inflection point (or the leading edge) of EDCs.

Fig. 3. STM of LBCO. (**A**) High-resolution STM topographic image of the cleaved sample. The image was taken at 4.2 K. (**B**) A tunneling conductance spectrum averaged over the area shown in (A). A v-like profile of DOS for energies $|\omega| \leq 20$ meV (gray region) is consistent with a d-wave gap observed in ARPES.
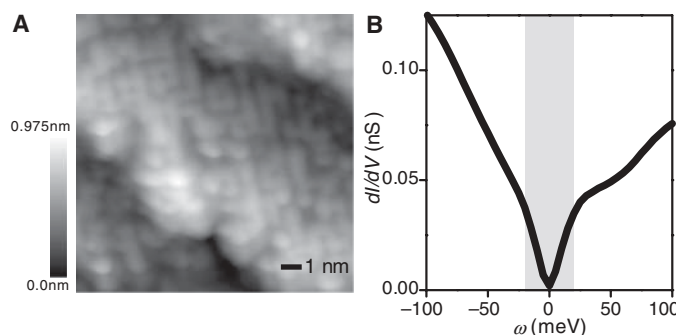

Fig. 4. A compilation of relevant wave vectors from neutron and x-ray scattering and ARPES on 214 materials. (**A**) A sketch of relevant vectors in the k-space. (**B**) Doping dependence of the antinodal k_F, indicated in (A) by the arrow, in LBCO (triangles) and LSCO (circle). The wave vector for charge order (13) (diamond) and the incommensurability δ from (π,π) point from neutron-scattering experiments (31, 32) (squares) are also shown. The gray vertical bar represents the boundary between the

"diagonal" and "parallel" spin superstructures and the onset of superconductivity. Error bars indicate fitting uncertainty in peak positions of MDC, used to extract k_F.
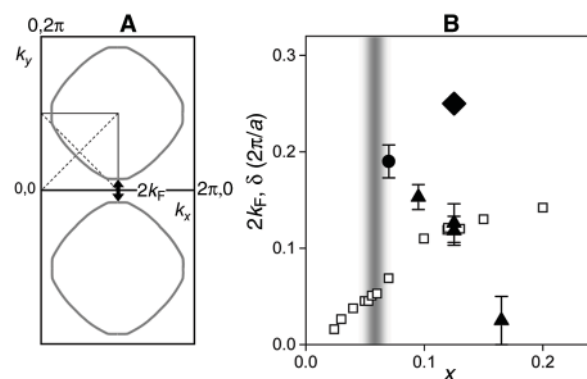
and a charge order (*12, 13*). Therefore, it would be tempting to assume that at least a portion of the measured gap is due to the charge order, in analogy with conventional two-dimensional (2D) charge density wave (CDW) systems. It has been suggested that, in cuprates, the spin-charge–ordered state forms in a way where carriers doped into the AF insulator segregate into 1D charge-rich structures (stripes) separated by the charge-poor regions of a parent antiferromagnet (*14, 23–25*). However, questions have often been raised on how to reconcile these unidirectional structures with an apparent 2D Fermi surface and a gap with *d*-wave symmetry. In the more conventional view, doped carriers are delocalized in the planes, forming a 2D Fermi surface that grows in proportion with carrier concentration. The charge-spin–ordered state may then be formed in the particle-hole channel by nesting of Fermi surface segments, producing a divergent electronic susceptibility and a Peierls-like instability and pushing the system into a lower energy state with a single-particle gap at nested portions of the Fermi surface. An example of a cuprate where such a "nesting" scenario is proposed to be at play is $Ca_{2−x}Na_xCuO_2Cl_2$ (CNCOC) (*26*). STM studies have detected checkerboard-like modulations in local DOS on the surface of this material, with $4a \times 4a$ periodicity, independent of doping (*27*). Subsequent ARPES studies on the same system have shown a Fermi surface with a nodal arc and truncated antinodal segments (*26*). The antinodal segments can be efficiently nested by the charge-ordering wave vectors $q_{CDW} = 2k_F = \pi/(2a)$ and $3\pi/(2a)$, observed in STM for charge superstructure, making the nesting scenario viable, at least near the surface of CNCOC. Here, k_F represents the antinodal Fermi wave vector. However, if we apply the same nesting scenario to LBCO at $x = \frac{1}{8}$, we obtain $q_{CDW} \approx 4k_F$ (= $\pi/2a$) for charge order instead of $2k_F$ nesting, which is suggested to be at play in CNCOC. Moreover, the nesting of antinodal segments would produce a wave vector that shortens with doping, opposite of that observed in neutron-scattering studies in terms of magnetic incommensurability. This result is illustrated in Fig. 4, where we compile the doping dependences of several relevant quantities.

There is another, more fundamental problem with the nesting scenario: Any order originating from nesting (particle-hole channel) would open a gap only on nested segments of the Fermi surface, preserving the non-nested regions. The fact that only four gapless points (nodes) remain in the ground state essentially rules out nesting as an origin of the pseudogap. In addition, a gap caused by conventional spin-charge order would be pinned to the Fermi level only in special cases. The observation that the gap is always pinned to the Fermi level (independent of *k*-point, as measured in ARPES and of doping level, as seen in STM on different materials) and that it has *d*-wave symmetry undoubtedly points to its pairing origin [interaction in the particle-particle singlet

channel (*28*)]. In contrast to the low-energy pairing gap, STM at higher energies shows a DOS suppressed in a highly asymmetric manner, indicating that some of the nesting-related phenomena might be at play at these higher energies (Fig. 3B).

The unexpected anticorrelation of the low-energy pairing gap and T_C over some region of the phase diagram suggests that, in the state with strongly bound Cooper pairs, the phase coherence is strongly suppressed by quantum phase fluctuations. Cooper pairs are then susceptible to spatial ordering and may form various unidirectional (*14, 24, 25*) or 2D (*15, 27–30*) superstructures. Quantum phase fluctuations are particularly prominent in cases where such superstructures are anomalously stable. For some of the proposed structures, this occurs at the doping of $\frac{1}{8}$, in general agreement with our results: $\frac{1}{8}$ represents the most prominent "magic fraction" for a checkerboard-like "CDW of Cooper pairs" (*15*), and it locks the stripes to the lattice in a unidirectional alternative. The presence of nodes in the ground state of the pseudogap represents a new decisive test for validity of models proposed to describe such structures.

References and Notes

1. T. Timusk, B. Statt, *Rep. Prog. Phys.* **62**, 61 (1999).
2. A. Damascelli, Z. Hussain, Z.-X. Shen, *Rev. Mod. Phys.* **75**, 473 (2003).
3. G. Baskaran, Z. Zou, P. W. Anderson, *Solid State Commun.* **63**, 973 (1987).
4. P. A. Lee, N. Nagaosa, X.-G. Wen, *Rev. Mod. Phys.* **78**, 17 (2006).
5. E. W. Carlson, V. J. Emery, S. A. Kivelson, D. Orgad, *The Physics of Superconductivity: Conventional and Unconventional*, vol. 2, K. H. Benneman, J. B. Ketterson, Eds. (Springer, Berlin, 2003).
6. M. Franz, Z. Tešanović, *Phys. Rev. Lett.* **87**, 257003 (2001).
7. V. J. Emery, S. A. Kivelson, *Nature* **374**, 434 (1995).
8. B. Lake *et al.*, *Science* **291**, 1759 (2001).
9. J. E. Hoffman *et al.*, *Science* **295**, 466 (2002).
10. M. Vershinin *et al.*, *Science* **303**, 1995 (2004).
11. K. McElroy *et al.*, *Phys. Rev. Lett.* **94**, 197005 (2005).
12. J. M. Tranquada *et al.*, *Nature* **429**, 534 (2004).
13. P. Abbamonte *et al.*, *Nat. Phys.* **1**, 155 (2005).
14. J. M. Tranquada, B. J. Sternlieb, J. D. Axe, Y. Nakamura, S. Uchida, *Nature* **375**, 561 (1995).
15. Z. Tešanović, *Phys. Rev. Lett.* **93**, 217004 (2004).
16. A. R. Moodenbaugh, Y. Xu, M. Suenaga, T. J. Folkerts, R. N. Shelton, *Phys. Rev. B* **38**, 4596 (1988).
17. C. C. Homes *et al.*, *Phys. Rev. Lett.* **96**, 257002 (2006).
18. X. J. Zhou *et al.*, *Phys. Rev. Lett.* **92**, 187001 (2004).
19. Materials and methods are available as supporting material on *Science* Online.
20. M. R. Norman *et al.*, *Nature* **392**, 157 (1998).
21. A. Kanigel *et al.*, *Nat. Phys.* **2**, 447 (2006).
22. M. Sutherland *et al.*, *Phys. Rev. Lett.* **94**, 147004 (2005).
23. J. Zaanen, O. Gunnarson, *Phys. Rev. B* **40**, 7391 (1989).
24. V. J. Emery, S. A. Kivelson, *Physica C* **235-240**, 189 (1994).
25. M. Granath, V. Oganesyan, S. A. Kivelson, E. Fradkin, V. J. Emery, *Phys. Rev. Lett.* **87**, 167011 (2001).
26. K. M. Shen *et al.*, *Science* **307**, 901 (2005).
27. T. Hanaguri *et al.*, *Nature* **430**, 1001 (2004).
28. M. Franz, *Science* **305**, 1410 (2004).
29. H.-D. Chen, O. Vafek, A. Yazdani, S.-C. Zhang, *Phys. Rev. Lett.* **93**, 187002 (2004).
30. D. Podolsky, E. Demler, K. Damle, B. I. Halperin, *Phys. Rev. B* **67**, 094514 (2003).
31. M. Fujita *et al.*, *Phys. Rev. B* **65**, 064505 (2002).
32. J. M. Tranquada *et al.*, *Phys. Rev. Lett.* **78**, 338 (1997).
33. The authors thank P. Anderson, A. Chubukov, E. Fradkin, C. Homes, P. Johnson, S. Kivelson, W. Ku, A. Millis, Z. Tešanović, A. Tsvelik, and J. Tranquada for useful discussions and Z-H. Pan for technical help. T.V., A.V.F., and G.D.G. are supported by the Office of Science, U.S. Department of Energy (DOE). J.C.D and J.L. are supported by the Office of Science, DOE, the Office of Naval Research, and by Cornell University.

Nondestructive Optical Measurements of a Single Electron Spin in a Quantum Dot

J. Berezovsky, M. H. Mikkelsen, O. Gywat, N. G. Stoltz, L. A. Coldren, D. D. Awschalom*

Kerr rotation measurements on a single electron spin confined in a charge-tunable semiconductor quantum dot demonstrate a means to directly probe the spin off-resonance, thus minimally disturbing the system. Energy-resolved magneto-optical spectra reveal information about the optically oriented spin polarization and the transverse spin lifetime of the electron as a function of the charging of the dot. These results represent progress toward the manipulation and coupling of single spins and photons for quantum information processing.

The prospect of quantum computation in conventional material systems has spurred much research into the physics of carrier spins in semiconductor quantum dots (QDs) (*1*).

Center for Spintronics and Quantum Computation, University of California, Santa Barbara, CA 93106, USA.

*To whom correspondence should be addressed. E-mail: awsch@physics.ucsb.edu

An important element necessary for spin-based quantum computing is the readout of the qubit spin state. Previously demonstrated schemes for single spin readout in a QD include optical measurements, such as photoluminescence (PL) polarization (*2, 3*) or polarization-dependent absorption (*4–6*). Single spins can also be read out electrically by measuring the spin-dependent probability for an electron to tunnel out of the